AIMS Bioengineering

AIMS Bioengineering, 13(1): 43–61.
DOI: 10.3934/bioeng.2026003
Received: 03 November 2025
Revised: 31 December 2025
Accepted: 26 January 2026
Published: 02 February 2026

https://www.aimspress.com/journal/Bioengineering

Research article

Real-time fatigue curve extraction algorithm for wearable sEMG devices based on fast variational mode decomposition

Tianshun Li[1,3], Donghao Lv[1,2,3,*], Dahua Yu[1,3], and Xiaowei Du[4]

[1] School of Automation and Electrical Engineering, Inner Mongolia University of Science and Technology, Baotou 014010, China
[2] School of Automation, China University of Geosciences, Wuhan 430074, China
[3] Key Laboratory of Synthetical Automation for Process Industries at Universities of Inner Mongolia Autonomous Region, Inner Mongolia University of Science and Technology, Baotou 014010, Inner Mongolia, China
[4] Department of Physical Education (Institute of Physical Education), Inner Mongolia University of Science and Technology, Baotou 014010, China

* **Correspondence:** Email: wsldh2016957@imust.edu.cn.

Abstract: Wearable devices are widely utilized in the field of health monitoring. Given the real-time requirements of wearable devices for dynamic tracking of muscle fatigue, and addressing the issues of prolonged computation time and failure to extract fatigue-related modal information when applying the variational mode decomposition (VMD) algorithm to surface electromyography (sEMG) signals, this paper proposes the fast VMD (FVMD) algorithm. The objective was to rapidly decompose fatigue-related modal information and extract a complete fatigue curve to alert users. The proposed algorithm is an engineering acceleration of the VMD algorithm. FVMD extends the original signal and applies the Fourier transform to convert the time-domain variational problem into the frequency domain. The optimization problem was constrained to the positive frequency range to simplify calculations while leveraging the unilateral spectrum characteristics to streamline optimization and focus on narrowband modes. The alternating direction method of multipliers framework was employed to decompose the problem into subproblems solvable in closed form, with modal updates inspired by Wiener filtering. The Lagrange multipliers were iteratively updated, and convergence criteria were established to ensure stability. The time-domain signal was reconstructed via the inverse Fourier transform. According to the experimental results, the proposed algorithm exhibits a substantial improvement in processing time compared to the original algorithm and other enhanced algorithms. Compared with other VMD variant

algorithms using the same experimental data, the fast recursive VMD (FRVMD) algorithm takes 9.93 s. In contrast, the FVMD method can complete the same task in a shorter time. An evaluation metric was used to select the muscle fatigue modal component most correlated with the original signal and extract the muscle fatigue curve. The FVMD algorithm enhances computational efficiency, overcoming the computational limitations of wearable devices, and provides reliable technical support for real-time muscle fatigue quantification and early warning in scenarios such as sports rehabilitation and occupational health.

Keywords: wearable devices; sEMG; fast variational mode decomposition; muscle fatigue curve

1. Introduction

Over the last few years, wearable devices have been used extensively in health care, fitness, and performance, among other sectors. Technological advancements have given recent achievements on bio-interfaces, neural-like collaborative control in intelligent prosthetic arms, electromyographic recognition of hand control in stroke victims, and wearable multi-modal human-machine interfaces in robotic arm control that show enormous promise in enhancing human health and life quality [1–3]. Wearable devices are widely used by connecting them directly to the human body, or they can be embedded within clothes, and they take advantage of high-level sensing technologies that can aid in constant tracking of physiological parameters. The combination of different sensors and processing units allows measuring the bio-signals, which helps to make the medical wearable technology miniaturized [4]. Such devices include wearable arrays of electrodes (or lots of electrodes), in particular flexible electronics, such as the inclusion ones, which prove to be highly applicable for dynamic fatigue monitoring in muscles. Muscle fatigue, referred to as the loss of force that results from prolonged or repetitive muscle contractions, is of great relevance in fields like sports training, rehabilitation, and medical diagnostics. The electrophysiological processes of muscle fatigue are observed mainly through a surface electrophysiological tool known as sEMG, which is a non-invasive technique by which the electrical activity of muscles is recorded by laying electrodes on the skin surface [5–7]. Nevertheless, sEMG signals are non-stationary, which complicates their processing because they are prone to noise and interference by other extraneous modal components [8]. Moreover, due to time-varying characteristics of sEMG signals, algorithms with high processing speed, real-time capabilities, and accuracy are required, especially when sEMG signals are applied to wearable devices in health monitoring. Therefore, the process of identifying a valuable feature of muscle fatigue and applying effective algorithms to resource-limited embedded systems is still a challenge in the field. Different signal processing techniques have been suggested to deal with such challenges. The types of techniques can be typically divided into: time-domain methods, frequency-domain methods, and time-frequency domain methods, with their respective pros and cons in being able to attend to the non-stationary and noisy nature of sEMG signals.

Time-domain signal processing processes work with the original signal, usually analyzed in terms of statistical features like the root mean square (RMS), zero-crossing rate, and mean absolute value (MAV). These approaches are both intuitive and computationally easy to implement, but struggle with the non-stationarity of sEMG signals, which may result in decreased robustness, particularly in the occurrence of noise. As an example, Goubault et al.'s study pointed out that time-domain features,

which include amplitude variations, may give information on muscle fatigue progression [9]. Likewise, as it was shown by Kim et al., such parameters as the zero-crossing rate and amplitude of muscle tension may be useful to describe muscle fatigue, but they depend on signal quality as well as the time window choice [10]. Özgören et al. set thresholds to screen dynamic signals for peaks, counting the frequency of peak events exceeding the threshold per unit time during continuous monitoring, and ultimately established a fatigue quantification model based on the time-varying characteristics of peak frequency [11]. Even though they are simple, time-domain approaches may be unable to process real-time data in challenging circumstances. Frequency-domain techniques, such as the Fourier transform, examine the signal as a comparison of frequency contents. They are useful in signals that contain stationary/periodic content, but are unable to detect the time-varying characteristic of non-stationary signals, such as sEMG. Fourier methods have been shown to provide information about the total muscle activity by examining the spectrum of power of the sEMG signal, although they do not give the possibility to observe the muscle fatigue progressively. These constraints especially become apparent with dynamically evolving or quickly changing signals, such as those in a wearable application. Time-frequency methods like wavelet transforms provide a more detailed method in that they offer both time and frequency information at the same time. This renders them with non-stationary signals such as sEMG. Such techniques as wavelet analysis have been applied to record dynamic variations in sEMG signals with regard to muscle fatigue [12–14]. Wavelet-based procedures, however, are subject to problems of subjective dispensation of basis functions, edge effects, and evaluation carry-ons. Although the use of wavelet transforms is a bit more flexible, the performance of the wavelet transform can be sensitive to parameters, hence differing in different applications. Modal decomposition methods have also been studied, including empirical mode decomposition (EMD) [15], which are able to break up non-stationary complex signals into simpler components known as intrinsic mode functions (IMFs) [16–19]. These techniques do not require subjectively choosing basis functions, which is a weakness of wavelet analysis. Huang et al. proposed EMD that enables the muscle fatigue to be studied in detail when intrinsic elements are extracted using sEMG signals [15]. On the same note, the VMD algorithm is a more advanced decomposition that offers better analysis and feature extraction, proposed by Dragomiretskiy et al. [20]. VMD has also been used in different tasks such as denoising and recognizing motion intention, and promising results have been shown in the analysis of sEMG signals [21–25]. Nonetheless, computational efficiency also presents problems to these approaches, and restricts their application in real-time in resource-constrained devices. Although the available signal processing techniques of sEMG signals provide useful information, they have their own limitations, which make them impossible to use in real-time in wearable devices. Time-domain techniques have problems with non-stationary signals, frequency-domain techniques cannot distinguish non-static changes, and time-frequency techniques can be computationally expensive. The modal decomposition techniques are useful and have the advantages of being computationally intensive and potentially inapplicable in real-time on wearable devices.

This paper will suggest a fast variational mode decomposition (FVMD) algorithm that resolves these problems by converting the variational problem to the frequency domain. The FVMD algorithm has a high computational efficiency, which allows the use of sEMG signals in real-time by the Fourier transform, and thus can use sEMG signals on wearable devices with resource constraints. The algorithm identifies the modal component that correlates with the original signal the most, according to the correlation coefficients and root mean square error, and extracts a full muscle fatigue curve by developing a linear expression fit. It is proven experimentally that the FVMD algorithm is able to

process sEMG signals much faster than the traditional VMD algorithms and extract muscle fatigue features.

The primary contributions of the paper are the following: (1) To meet the real-time processing needed for wearables, we propose the FVMD algorithm, a processing algorithm that takes much less time to process sEMG signals. (2) Muscle fatigue features extraction: The FVMD algorithm can successfully extract a whole muscle fatigue profile of the sEMG signals by applying the methods of power spectral density analysis and linear fitting.

The structure of this paper is as follows: After this section, Section 2 introduces the basic principles, formula derivation, and process flow of the algorithm. Section 3 uses laboratory-measured sEMG signals to test the performance of the proposed algorithm. Section 4 summarizes the content of this paper.

2. Materials and methods

2.1. Proposed method

First, construct the non-stationary nonlinear signal function expression $f(t) \in R,\ t \in [0,T]$. $f(t)$ denotes the value of the original signal at time t. To reduce boundary problems caused by spectral leakage and periodic convolution effects, mirror extension is performed on the original signal. Mirror extension makes the signal continuous at the boundary, reducing the discontinuity caused by the periodicity assumption of the Fourier transform, concentrating the spectrum, and reducing high-frequency noise interference.

$$f_{\text{mirror}}(t) = \left[f\left(\frac{T}{2}:-1:1\right),\quad f(t),\quad f\left(T:-1:\frac{T}{2}+1\right)\right] \tag{1}$$

Among them, $\frac{T}{2}{:}{-}1{:}1$ indicates that the first half of the original signal is inverted, and $T{:}{-}1{:}\frac{T}{2}{+}1$ indicates that the second half of the original signal is inverted. A Fourier transform is performed on the extended signal to obtain its frequency domain representation. $f_{mirror}(t)$ is the new sequence, which is the result of the mirror extension of the initial signal. T denotes the total length of the signal.

$$\hat{f}(\omega) = \mathcal{F}\{f_{\text{mirror}}\}(\omega),\quad \omega \in \left[-\frac{1}{2},\frac{1}{2}\right] \tag{2}$$

We convert the time-domain signal to the frequency domain to lay the foundation for subsequent frequency-domain optimization. We extend the original signal, perform a Fourier transform on it, and convert the time-domain variational problem of the VMD algorithm to the frequency domain. This is the key to the fast processing of the algorithm proposed in this paper. We convert the time-consuming time-domain convolution operation to the frequency domain for operation. $\hat{f}(\omega)$ is the frequency representation of the signal. In particular, it refers to the spectrum that is acquired following the mirror extension of the signal after the Fourier transform is applied to the signal. ω denotes the normalized frequency variable. $F\{\cdot\}$ is the Fourier transform operator, whose role is to convert a signal in the time arena to the frequency arena, and thus get its spectral representation.

The core of the VMD algorithm is based on the analytic signal. For a real-valued signal $u_k(t)$, the

Fourier transform $\hat{u}_{k,A}(\omega)$ of its analytic signal $u_{k,A}(t) = u_k(t) + j\mathrm{H}\{u_k(t)\}$ has a one-sided spectral characteristic, i.e., for ω < 0, $\hat{u}_{k,A}(\omega) = 0$. Therefore, the one-sided spectrum $\hat{f}^{+}(\omega)$ of the signal is extracted. + means that the positive component is retained only.

$$\hat{f}^{+}(\omega) = \begin{cases} 2\hat{f}(\omega), & \omega > 0 \\ \hat{f}(0), & \omega = 0 \\ 0, & \omega < 0 \end{cases} \tag{3}$$

Convert the signal into an analytic form so that its spectrum is concentrated on the positive frequency axis, limiting the optimization problem to the positive frequency range and simplifying subsequent calculations.

The goal of VMD is to decompose the signal *f(t)* into *K* modes such that each mode has a compact spectrum near its center frequency and the sum of all modes can reconstruct the original signal.

$$\min_{\{u_k\},\{\omega_k\}} \left\{ \sum_{k=1}^{K} \left\| \partial_t \left[(u_k(t) + j\mathcal{H}\{u_k(t)\}) e^{-j\omega_k t} \right] \right\|_2^2 \right\} \qquad \text{s.t.} \quad \sum_{k=1}^{K} u_k(t) = f(t) \tag{4}$$

$u_k(t)$ represents the *K*th modal function. ω_k is the center frequency of the *K*th mode, which is the position where this mode is dominant in the spectrum. $e^{-j\omega_k t}$ is the exponential factor of the complex number used to shift the signal to the frequency band centered on ω_k. $\mathrm{H}\{u_k(t)\}$ performs the Hilbert transform on the modal $u_k(t)$. ∂_t denotes the derivative with respect to time *t*. $u_{k,A}(t) = u_k(t) + j\mathrm{H}\{u_k(t)$ is the analytical signal of the *k* modal $u_k(t)$, $u_k^{\text{base}}(t) = u_{k,A}(t)e^{-j\omega_k t}$ is the signal obtained by shifting the spectrum of the analytical signal to the baseband, $\|\cdot\|_2^2$ represents the L^2 norm, ∂_t represents the time derivative, and $\|\partial_t u_k^{\text{base}}\|_2^2$ measures the smoothness of the baseband signal. The objective function is constructed in the frequency domain, and the above-mentioned time-domain objective function is converted to the frequency domain form. Based on Parseval's theorem, the properties of frequency domain differentiation, and the properties of frequency domain shifting, these properties can be substituted into the bandwidth constraint term to obtain:

$$\min_{\{u_k\},\{\omega_k\}} \left\{ \sum_{k=1}^{K} \frac{1}{2\pi} \int_0^{\infty} (\omega - \omega_k)^2 \, |\, \hat{u}_k^{+}(\omega) \,|^2 \, d\omega \right\} \qquad \text{s.t.} \quad \sum_{k=1}^{K} \hat{u}_k^{+}(\omega) = \hat{f}^{+}(\omega) \tag{5}$$

$\widehat{u_k^{+}}(\omega)$ in the equation above represents the unilateral spectrum of the *k*th mode, which is obtained as a result of signal decomposition. $\widehat{f^{+}}(\omega)$ represents the unilateral spectrum of the original signal. $|\widehat{u_k^{+}}(\omega)|^2$ represents the spectral power density of the *k*th mode. We convert complex time-domain derivatives and convolution operations into simple mathematical operations in the frequency domain, thereby preparing for subsequent alternating direction method of multipliers (ADMM) optimization operations. To solve constrained variational problems, the Lagrange method is introduced.

$\mathcal{L}$ denotes the Lagrange function. $\{u_k\}$ represents the set of modal functions. $\{\omega_k\}$ denotes the set of modal center angular frequencies. $\partial_t u_k^{base}$ indicates the first derivative with respect to time of the modal fundamental analytical signal. $<\cdot>$ is the symbol of the inner product, which is the dot product of two functions.

By introducing the Lagrange multiplier λ(t) and the quadratic penalty term α, the constraint terms are incorporated into the objective function, thereby obtaining the time-domain objective function:

$$\mathcal{L}(\{u_k\},\{\omega_k\},\lambda)=\alpha\sum_{k=1}^{K}\left\|\partial_t u_k^{\text{base}}\right\|_2^2+\left\|f(t)-\sum_{k=1}^{K}u_k(t)\right\|_2^2+\left\langle\lambda(t),f(t)-\sum_{k=1}^{K}u_k(t)\right\rangle \tag{6}$$

Further, we convert the time-domain function to the frequency domain to obtain the objective function in the frequency domain form. $\widehat{\lambda^+}$refers to the depiction of the Lagrange multiplier in the unilateral frequency domain in this equation. R(·) denotes the real part. $\widehat{f^+}$ represents the unilateral spectrum of the original signal.

$$\mathcal{L}=\alpha\sum_{k=1}^{K}\int_0^{\infty}(\omega-\omega_k)^2\,|\hat{u}_k^+(\omega)|^2\,d\omega+\left\|\hat{f}^+-\sum_{k=1}^{K}\hat{u}_k^+\right\|_2^2+\Re\left\langle\hat{\lambda}^+,\hat{f}^+-\sum_{k=1}^{K}\hat{u}_k^+\right\rangle \tag{7}$$

We convert the constrained problem into an unconstrained problem to prepare for ADMM iterative solving.

The ADMM is used to iteratively update $\{u_k^+\}$、$\{\omega_k\}$, and λ^+. To update the spectrum $\hat{u}_k^+(\omega)$ of the *k*th mode, we fix the other modes $\hat{u}_j^+(\omega)\,(j\neq k)$, center frequency ω_k, and Lagrange multiplier $\hat{\lambda}^+(\omega)$. The objective is to minimize a part of $\hat{u}_k^+(\omega)$, thereby obtaining the update formula for $\hat{u}_k^+(\omega)$ as follows:

$$\hat{u}_k^{n+1}(\omega)=\frac{\hat{f}^+(\omega)-\sum_{i\neq k}\hat{u}_i^n(\omega)+\frac{\hat{\lambda}^n(\omega)}{2}}{1+\alpha(\omega-\omega_k^n)^2} \tag{8}$$

In the above equation, $\widehat{u_k^{n+1}}(\omega)$ denotes the frequency domain representation of the *K*th mode at the $n+1$ iteration. $\widehat{\lambda^n}(\omega)$ is a shape of the Lagrange multiplier in the frequency domain. The denominator is a frequency-responsive function that attenuates frequency components far from the center frequency ω_k, thereby narrowing the bandwidth of the mode. The numerator is the residual signal obtained by subtracting other modes and the Lagrange multiplier from the original signal. To update the center frequency ω_k of the mode, fix mode $\hat{u}_k^+(\omega)$ and Lagrange multiplier $\hat{\lambda}^+(\omega)$. The updated formula for ω_k is obtained as follows:

$$\omega_k^{n+1}=\frac{\int_0^{\infty}\omega\left|\hat{u}_k^{n+1}(\omega)\right|^2 d\omega}{\int_0^{\infty}\left|\hat{u}_k^{n+1}(\omega)\right|^2 d\omega} \tag{9}$$

ω_k^{n+1}represents the center frequency of the *K*th mode at the $n+1$ step. This equation shows that the center frequency of a mode is the weighted average of its power spectrum, which is the center of gravity of the power spectrum. This intuitively captures the frequency position where the mode energy is most concentrated.

$\lambda^n(t)$ and $\lambda^{n+1}(t)$ denote the values of the Lagrange multiplier at time *t* during the *n*th and (*n*+1)th iterations, respectively. τ is the updating step, and is used to control the speed with which the Lagrange multiplier is updated. $\sum_{k=1}^{K}u_k^{n+1}(t)$ is the superposition of *K* modal functions obtained at the $n+1$ iteration. The Lagrangian multiplier update of the time domain signal function is

$$\lambda^{n+1}(t)=\lambda^n(t)+\tau\left(f(t)-\sum_{k=1}^{K}u_k^{n+1}(t)\right) \tag{10}$$

We construct frequency domain Lagrange multiplier updates based on equation (10):

$$\hat{\lambda}^{n+1}(\omega) = \hat{\lambda}^{n}(\omega) + \tau\left(\hat{f}^{+}(\omega) - \sum_{k=1}^{K}\hat{u}_k^{n+1}(\omega)\right) \tag{11}$$

where τ is the step size of the Lagrange multiplier update and $\hat{\lambda}^{+}(\omega)$ is responsible for correcting the reconstruction error of the signal during the iteration process. If there is a difference between the current modal sum and the original signal, the Lagrange multiplier will be adjusted accordingly to reduce this difference in the next iteration. By iteratively updating the Lagrange multiplier to enforce the reconstruction constraint and using the relative change as the convergence criterion, the robustness and stability of the algorithm are ensured.

Modal spectrum symmetry constraint: Since the original signal *f(t)* must have a Fourier transform $\hat{f}(\omega)$ that satisfies conjugate symmetry $\hat{f}(\omega) = \hat{f}^{*}(-\omega)$, each mode $u_k(t)$ is also real-valued, and its spectrum $\hat{u}_k(\omega)$ must satisfy this property as well. During ADMM iterations, only the unilateral spectrum $\hat{u}_k^{+}(\omega)$ of the positive frequency component is updated, which is then used to reconstruct the negative frequency part.

$$\hat{u}_k(\omega) = \begin{cases} \hat{u}_k^{+}(\omega) & \omega \geq 0 \\ \mathrm{conj}(\hat{u}_k^{+}(-\omega)) & \omega < 0 \end{cases} \tag{12}$$

To determine whether the algorithm converges, the relative change in all modal spectra in consecutive iterations is typically calculated.

$$\Delta = \frac{\sum_{k=1}^{K} \| \hat{u}_k^{n+1} - \hat{u}_k^{n} \|_2^2}{\sum_{k=1}^{K} \| \hat{u}_k^{n} \|_2^2 + \epsilon} \tag{13}$$

where ε is an infinitesimal positive number approaching zero to prevent division by zero. If Δ is less than the preset tolerance, the algorithm is considered to have converged and the iteration stops.

Signal reconstruction: Once the algorithm converges, the frequency-domain representation of each mode can be obtained, and the time-domain mode $u_k(t)$ can be derived through an inverse Fourier transform.

$$u_k(t) = \Re\left\{\mathcal{F}^{-1}\left[\hat{u}_k(\omega)\right]\right\} \tag{14}$$

Since the input signal *f(t)* has undergone mirror extension, the final *(t)* btained is also the extended length. We cut out the part corresponding to the length of the original signal based on the length of the extension.

The determination of the fixed number of modes and penalty term settings used in this study was based on the nature of the signal and previous experiments. Namely, the mode selection was based on the spectral characteristics and complexity of the signal, and the medium value was chosen to enable efficient decomposition of the signal without requiring excessive computational resources. The risk of overfitting was mitigated by the penalty term, resulting in a smooth decomposition that could be interpreted as needed. The primary objective of this methodology is to simplify the algorithm in experimental conditions, reduce computational cost, and achieve a high processing speed. This is especially important in practice, where large volumes of signal data have to be processed quickly.

In the frequency domain implementation of FVMD, many operations are performed directly in the frequency domain, resulting in higher actual efficiency. Its core advantage lies in the fact that modal updates no longer require time domain convolution, but are instead processed in the frequency domain, which greatly improves the processing efficiency of the algorithm.

2.2. Experimental subjects and data collection

The citizens chosen for the experiment were between the ages of 23 and 26 years. A male standard of 175.0 ± 5.0 cm was used as the height standard for the male participants, and the female stakeholders used a height standard of 158.0 ± 3.0 cm. Each respondent was examined for their health and was determined to be normal in terms of skeletal, muscular, and nerve conditions. The subjects were not allowed to exercise for 24 hours prior to the experiment. Every participant was provided with adequate information regarding the experiment's intent, procedures, and possible risks, and signed an informed consent form. The RTLab software platform, featuring the RunE series of wireless physiological signals acquisition terminals, was utilized as a data collection tool produced by Shenzhen Runyi Taiyi Technology Co., Ltd. The frequency at which the system was sampled was 1000 Hz. The analysis of the data and the creation of the algorithm were performed using a laptop terminal that has the Intel i7-13620H processor, RTX4050, with a clock speed of 4.90 GHz (GPU) and the Windows 11 operating system. Computational computations were done in MATLAB R2024a. This was done in the Data Sensing and Analysis Laboratory. Technicians applied 75% medical-grade alcohol swabs to the area of the brachioradialis muscle of the subject and ensured that the skin impedance met the data collection requirements during the pre-operation preparation stage. The sitting posture was standard, where the trunk was perpendicular to the ground, the upper arm was horizontally abducted parallel to the trunk, the forearm naturally hung to make a 90-degree elbow joint angle, and one hand gripped a 3-kilogram standard dumbbell. Following the onset of the experiment, the target controlled the stability of the dumbbell using isometric contractions of the brachioradialis muscle until the subject noted brevity or incapacity to hold the position, which indicated the end of data collection.

To further explore the performance of the algorithm when applied to non-isometric movements, an experiment on grip strength was conducted in this part. This enhances the usability of the algorithm for wearable devices with dynamic and varying muscular engagement. The conditions for all experimental personnel, environment, and equipment were the same as before. Before the experiment, the palmaris longus area of each subject was disinfected and degreased by technicians using 75% medical-grade alcohol, ensuring the skin impedance met the experiment's requirements. The subject sat upright with their back against the chair, the head of the upper arm against their torso, and their forearm at 90 degrees to their upper arm. They held the dynamometer with one hand. Upon commencement, the subject gripped the dynamometer with maximum force for several seconds before releasing. After a brief relaxation period, they resumed gripping. This cycle was repeated until the subject reported arm fatigue, rendering further gripping impossible.

2.3. sEMG pre-processing

Figure 1 shows the sEMG signal to be analyzed. The effective information is mainly concentrated in the 10–500 Hz range. To avoid power frequency interference, this study used a 10–500 Hz bandpass filter to pre-process the surface electromyography signal and reduce noise interference. To facilitate

subsequent data analysis, the sampling frequency was set to 1000 Hz. The data used includes 68,350 signal data points, which comprehensively cover the entire muscle fatigue process.

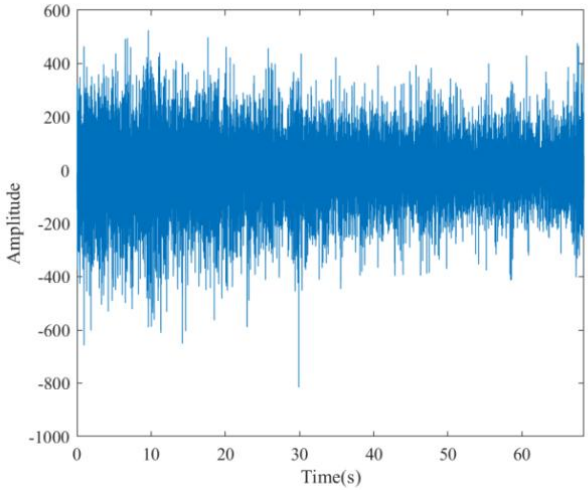

Figure 1. Raw pre-processed sEMG signals collected.

Figure 2 displays the grip strength sEMG signals obtained during the experiment. To minimize interference from extraneous information, the sEMG signals underwent pre-processing. The sampling rate was adjusted to 2000 Hz, and a total of 137,790 data points were used, which were fully interpolated across the entire range of the activity cycle between the non-fatigued state and the fatigued state of the subjects.

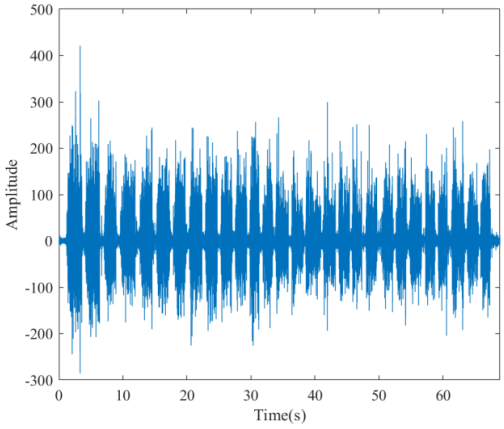

Figure 2. sEMG grip strength time domain waveform.

2.4. Evaluation metrics

Furthermore, based on these spectral properties, the median frequency (MDF) has been used as a modal screening criterion to further optimize the modal selection process of components, thereby enhancing the representation of nonlinear dynamic properties of muscle fatigue and providing good

physiological interpretability. To relate all of these spectral properties to the analytical rigor, quantitative screening criteria were later developed to identify effective mode components that exhibit properties of muscle fatigue, providing a reliable basis for future analyses.

$$MDF = \frac{1}{2}\int_0^{\infty} PSD(f)df \tag{15}$$

3. Results

3.1. sEMG experimental findings during sustained effort

This study used laboratory-measured surface electromyography signals to validate the algorithm. The processing time of the FVMD algorithm was 3.51 s, which is 13 times faster than the 45.68 s required by the traditional VMD algorithm in terms of computational efficiency. Under the same data and experimental conditions, the fast recursive VMD (FRVMD) [26] algorithm took 9.93 s. Compared with other variants of the VMD algorithm, the computational efficiency was improved by 2.82 times. When decomposing the sEMG obtained from subjects who continuously contracted until exhaustion, the FVMD algorithm stably generated five eigenmode components, as shown in Figure 2.

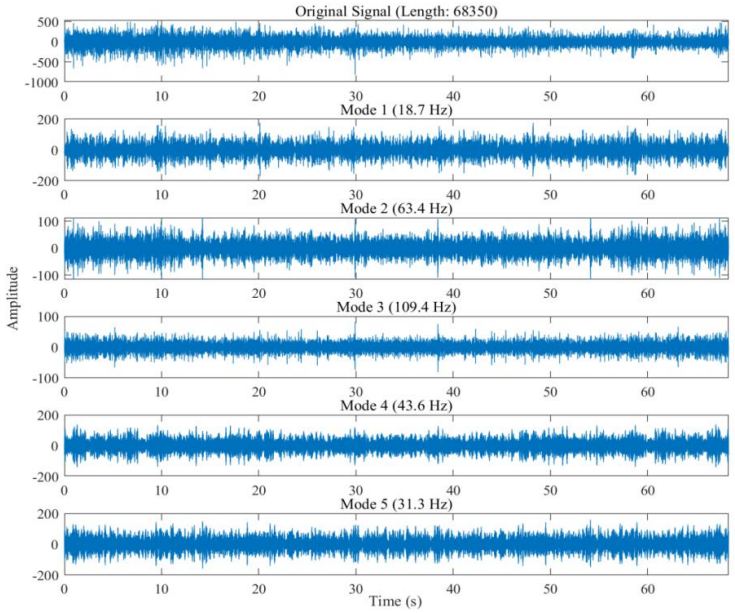

Figure 3. Sub-modal signals decomposed after processing by the FVMD algorithm.

As shown in Figure 3, the time-domain waveforms of each mode exhibit significant differences: mode 3 exhibits high-frequency oscillations with frequencies exceeding 100 Hz, representing the high-frequency oscillatory components of single muscle fiber action potentials. Mode 1, mode 4, and mode 5 exhibit low-frequency oscillations with frequencies below 50 Hz, reflecting motor unit recruitment synchronization and the overall activation state of the muscle. Mode 2 exhibits medium-frequency oscillations with frequencies between 50 Hz and 150 Hz, which are related to the muscle fiber conduction velocity and motor unit discharge rate. These modes fully cover the physiological frequency range of the sEMG signal.

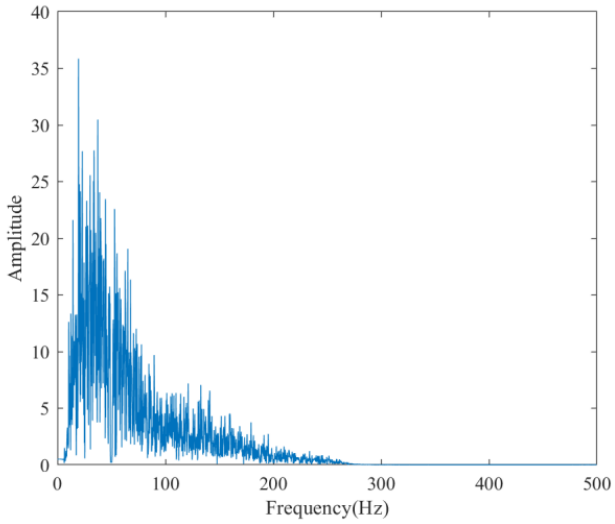

Figure 4. Spectrum diagram.

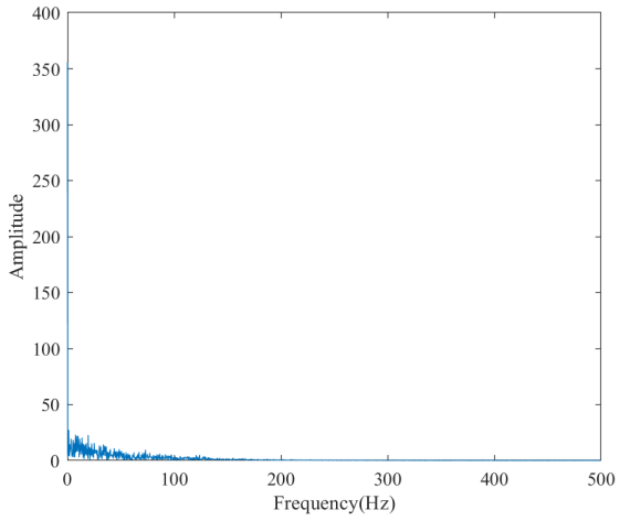

Figure 5. Envelope spectrum.

As shown in Figure 4, the frequency spectrum of the sEMG signal shows low-frequency dominance of the signal, with progressive attenuation of data at higher frequencies, a characteristic pattern of muscular activity. Such spectral properties reflect the recruitment strategy and metabolic state of the motor units during contraction. During the first contraction cycle, the use of fast-twitch fibers therefore adds a disproportionate amount of high-frequency energy. When contraction continues, the spectral centroid moves downward because the velocity of such fibers reduces due to fatigue caused by metabolic activity. This decreasing trend is a salient indicator of muscle fatigue. Figure 5 will show variations in the intensity of muscle activity in which the energy table of sEMG signals is positively related to the contraction force. An increase in force will activate more motor units, thus raising the amplitude; conversely, the less force applied, the lower the amplitude. Therefore, the energy distribution of the envelope spectrum becomes a sensitive indicator of the muscle's condition. Through

the combination of spectral and envelope analysis, a multidimensional, synchronized characterization of muscle response can be attained, further enabling us to gain a better insight into the physiological process underlying it.

Calculations showed mode 1 of 19.5 Hz, mode 2 of 62.5 Hz, mode 3 of 106.4 Hz, mode 4 of 43.9 Hz, mode 5 of 41.2 Hz, and mode 4 was chosen to analyze. This indicates that mode 4 retains a significant amount of physiological information from the original signal and is suitable as a carrier for fatigue feature extraction.

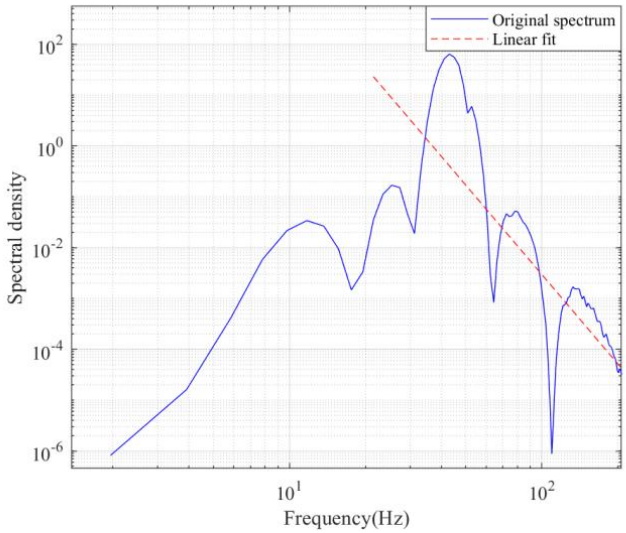

Figure 6. Spectral slope analysis.

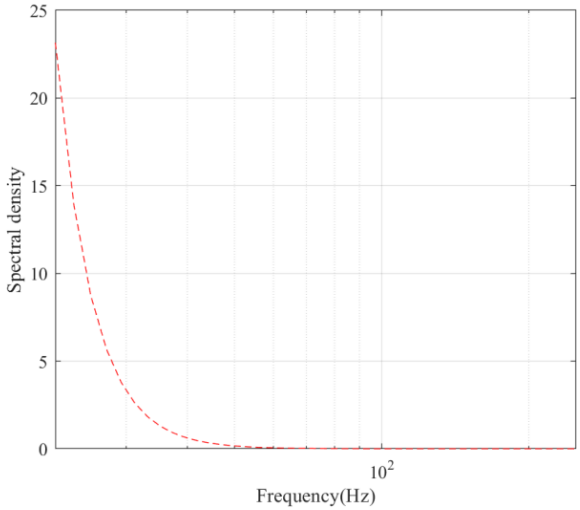

Figure 7. Linear fitting in logarithmic coordinates.

We performed a power spectral density (PSD) analysis of the chosen mode. After extracting the PSD of the signal, we found the original spectrum and the fitted line in a double-log coordinate system. Figure 6 shows that the frequency range of the linear relationship of surface electromyography (sEMG)

is strong (15 to 200 Hz). In this regime, spectral attenuation exhibits a strong linear shape, with a fitted slope of −5.83, indicating an exponential decay in modal energy with increasing frequency. The magnitude of the slope transmits the rate of attenuation of the spectral energy. The negative value indicates that high-frequency energy fades faster than the low-frequency components, and this fact can be explained by two physiological processes, namely, a fatigue-related decrease in the conduction velocity of the action potentials that lowers a portion of the high-frequency energy, and simultaneously, an improved motor unit synchronization that increases a share of the low-frequency energy. The PSD of mode 4 displays erratic attenuation traits in the dual log coordinates shown in Figure 7. The acquired muscle fatigue curves were cross-tested with the Borg RPE Scale, and it was proven that the two have a high level of correlation. The fatigue curve, obtained after optimizing the relevant equation, has far-reaching implications for physiological health research. Loss of high-frequency components is directly proportional to the loss of muscle fiber conduction velocity. Rising action potential time significantly decreases high-frequency oscillatory energy. During fatigue, the nervous system recruits more motor units to maintain force output, leading to synchronized discharge efficiency, a reduced discharge rate, and decreased discharge frequency of individual motor units. This power-law characteristic provides a new metric for quantifying fatigue.

3.2. Intermittent effort sEMG experimental results

In this part, non-uniform motion grip sEMG signals were utilized to evaluate the proposed algorithms. Empirical evidence shows that the FVMD algorithm had a processing time of 6.63 seconds, the FRVMD algorithm an average processing time of 8.54 seconds, and the VMD algorithm an average processing time of 10.17 seconds. This is a 1.3-fold and 1.5-fold increase in computational efficiency, respectively. The FVMD algorithm processed the grip force signal decomposition to generate five modes, as illustrated in Figure 8.

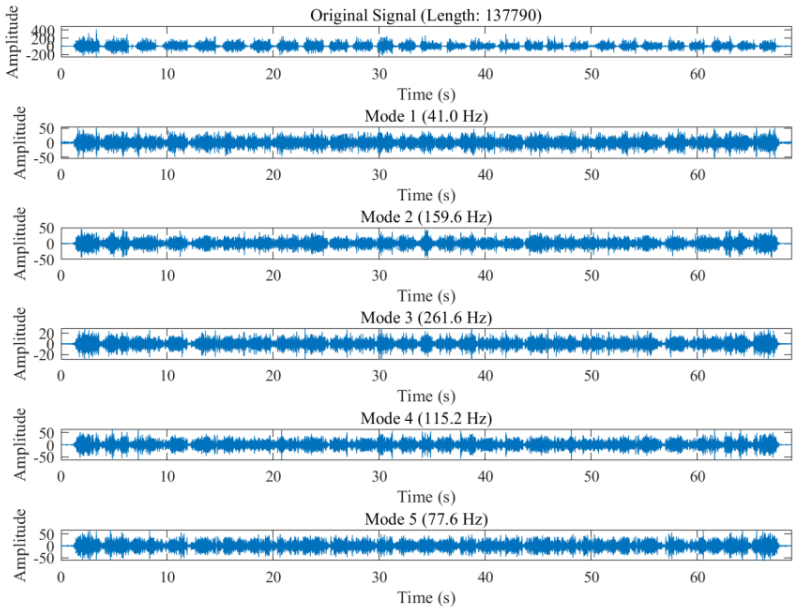

Figure 8. Grip force signal following FVMD algorithm decomposition.

As illustrated in Figure 8, different modes present distinct information. Mode 1 exhibits a central frequency within the time domain. In this mode, amplitude fluctuations are relatively smooth. The energy distribution is also comparatively uniform. Mode 2 and mode 3 have central frequencies within the 100–300 Hz range of the electromyographic signal. In the time domain plot, both their frequency and amplitude fluctuations exceed those of mode 1. The central frequency of mode 4 is between 100 and 120 Hz. This is an activity at the rapid rise period of muscle tension. Mode 5 has less rapid changes in the amplitude of the central frequency.

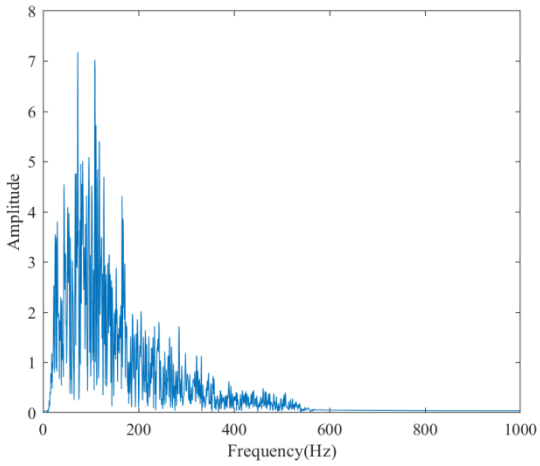

Figure 9. Spectrum diagram.

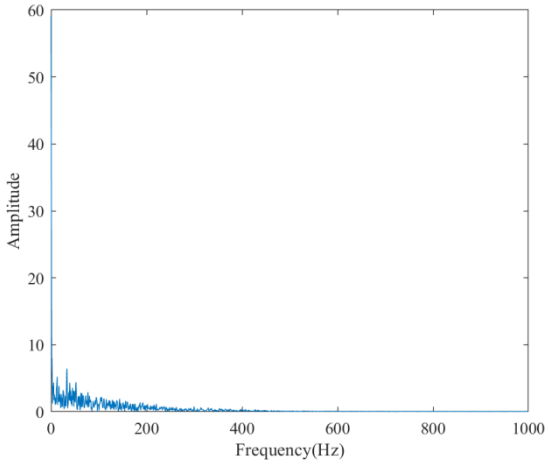

Figure 10. Envelope spectrum.

The spectral diagram shows that the energy distribution is unequal. Most effective energy is concentrated in the low- and mid-frequency ranges. There is a sharp drop in signal to zero beyond these, especially above 400 Hz. This illustrates the rate of motor unit discharge, the properties of action potential waveforms, and the conduction properties in tissue. In the core frequency band where energy is concentrated, several fluctuating peaks are visible. This typically corresponds to the frequency range of the main discharge of motor units and muscle contraction. During dynamic, non-isometric

movements, as muscle length and contraction velocity change, the recruitment pattern and release rate of motor units also change. This results in a more scattered spectral profile compared to isometric contractions. The numerous peaks might accurately reflect this dynamic regulatory process.

Following these results, we analyzed the information using the MDF. The measured frequencies were: mode 1 (39.1 Hz), mode 2 (144.5 Hz), mode 3 (242.2 Hz), mode 4 (105.5 Hz), and mode 5 (74.2 Hz). Based on these results, mode 1 was selected as the subject for analysis.

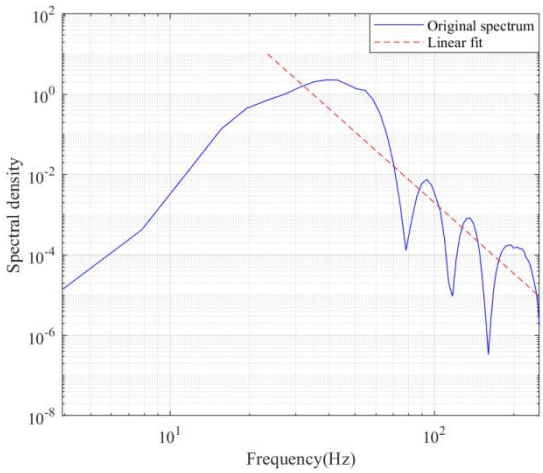

Figure 11. Spectral slope analysis.

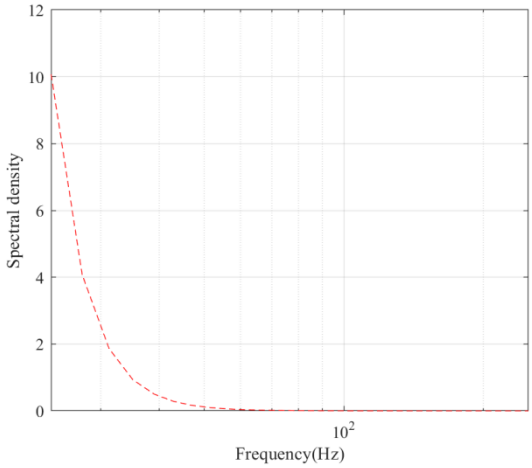

Figure 12. Linear fitting in logarithmic coordinates.

As can be observed from the figure above, during the fatigue process induced by intermittent grip strength, the sEMG power spectrum exhibits a well-defined near-linear decay within the 15–200 Hz range, with a fitted slope of −5.87. Cross-validation using the Borg RPE Scale was also performed in this section, and it proved that the suggested method reveals physiological validity. Power-law fitting in a double-logarithmic coordinate system does more than just give a visual representation of the spectral characteristics of fatigue, but also condenses them into similar quantitative measures. This makes it usable in physiological health monitoring as well as the performance validation of algorithms.

4. Conclusions

This study presents an innovative approach to health monitoring using wearable devices by introducing a novel FVMD algorithm. The proposed method enhances the ability of wearable devices to monitor muscle fatigue more efficiently. By optimizing the processing workflow, the FVMD algorithm improves the processing speed of sEMG signals, offering a promising solution to the technical challenges of real-time monitoring in constrained wearable environments. While the experimental results indicate that the FVMD algorithm captures the muscle fatigue process effectively, extracting a comprehensive fatigue curve and facilitating a more robust quantitative assessment, further validation across a broader range of conditions is necessary. The improvements in processing speed, reported to be 13 times faster than traditional VMD algorithms, are significant; however, the study acknowledges the need for a larger experimental dataset and statistical validation to confirm the generalizability of the results across diverse populations and activity conditions. Although this study showcases the potential of the FVMD algorithm in overcoming resource limitations in wearable devices and its applicability to lightweight, real-time performance, it is important to note that the current findings are based on a limited set of experiments. The results should be considered preliminary, and further studies, including larger trials and comparisons with alternative methods, are essential to strengthen the credibility of these findings. Looking ahead, the integration of deep learning techniques with multi-channel sEMG signal fusion analysis is a promising direction for future research. This could not only refine the accuracy of fatigue detection but also open avenues for broader applications in muscle fatigue monitoring, making it more suitable for diverse real-world scenarios. Nevertheless, the current study provides a solid foundation for these future explorations, while emphasizing the importance of continued research and development to establish the long-term feasibility and accuracy of these methods.

Use of AI tools declaration

The authors declare they have not used Artificial Intelligence (AI) tools in the creation of this article.

Acknowledgments

This research received partial funding from the Natural Science Foundation of the Inner Mongolia Autonomous Region (2024MS06024), the Special Fund for Basic Research Operations at Inner Mongolia University of Science and Technology (2023QNJS194), and the Special Research Project for the First-Level Discipline of Metallurgical Engineering from the Department of Education of the Inner Mongolia Autonomous Region (YLXKZX-NKD-020).

Conflict of interest

The authors declare no conflict of interest.

Author contributions

All authors contributed to the conceptualization and design of the study. Material preparation and data analysis were performed by Tianshun Li and Donghao Lv. Tianshun Li completed the initial draft and experimental work. Dahua Yu provided experimental guidance, while Xiaowei Du contributed data support. All authors reviewed earlier versions of the manuscript. All authors read and approved the final manuscript.

Novelty claim

The proposed algorithm is an engineering acceleration of the VMD algorithm.

Ethics approval of research

The Ethics Committee of the People's Hospital of Linhe District, Bayannur City, approved all procedures. All individual participants in the study provided informed consent and obtained a paper-based informed consent form.

References

1. Lu Z, Zhou Y, Huang Q, et al. (2024) A motion control method for robotic arm based on a wearable hybrid human-machine interface. *Robot* 46: 68–80. https://doi.org/10.13973/j.cnki.robot.230254
2. Li J, Zhang B, Yao J, et al. (2022) Biomechanical interface system and neural-like cooperative control for the intelligent prosthetic arm. *Robot* 44: 546–563. https://doi.org/10.13973/j.cnki.robot.220156
3. Hu S, Zhang D, Zhao X, et al. (2021) An sEMG-based hand motion recognition method for stroke patients with feature engineering and cascade forest. *Robot* 43: 526–538. https://doi.org/10.13973/j.cnki.robot.200588
4. Jegan R and Nimi W (2024) On the development of low power wearable devices for assessment of physiological vital parameters:a systematic review. *J Public Health* 32: 1093–1108. https://doi.org/10.1007/s10389-023-01893-6
5. Zhu Y, Lv D, Zhang Y (2022) Classification method of sEMG based on improved model. *Electr Eng* 8: 67–69. https://doi.org/10.19768/j.cnki.dgjs.2022.08.022
6. Yao H, Lv D, Zhang Y, et al. (2023) Study of muscle fatigue state classification based on fourier decomposition method. *J Electron Meas Instrum* 37: 48–58. https://doi.org/10.13382/j.jemi.B2306358
7. Cao Z, Lv D, Zhang Y, et al. (2024) Muscle fatigue classification based on geometric features of sEMG signal. *Transducer Microsyst Technol* 43: 145–148. https://10.13873/J.1000-9787(2024)07-0145-04
8. Xi K, Lv D, Yang C, et al. (2025) Adaptive bandwidth chirp mode decomposition for muscle fatigue analysis. *Measurement* 257: 118679. https://doi.org/10.1016/j.measurement.2025.118679

9. Goubault E, Martinez R, Bouffard J, et al. (2022) Shoulder electromyography-based indicators to assess manifestation of muscle fatigue during laboratory- simulated manual handling task. *Ergonomics* 65: 118–133. https://doi.org/10.1080/00140139.2021.1958013
10. Kim H, Lee J, Kim J. (2018) Electromyography-signal-based muscle fatigue assessment for knee rehabilitation monitoring systems. *Biomed Eng Lett* 8: 345–353. https://doi.org/10.1007/s13534-018-0078-z
11. Özgören N and Aritan S (2022) Peak counting in surface electromyography signals for quantification of muscle fatigue during dynamic contractions. *Med Eng Phys* 107: 103844. https://doi.org/10.1016/j.medengphy.2022.103844
12. Shariatzadeh M, Hadizadeh Hafshejani E, Mitchell C, et al. (2023) Predicting muscle fatigue during dynamic contractions using wavelet analysis of surface electromyography signal. *Biocybern Biomed Eng* 43: 428–441. https://doi.org/10.1016/j.bbe.2023.04.002
13. Daniel N, Małachowski J, Sybilski K, et al. (2024) Quantitative assessment of muscle fatigue during rowing ergometer exercise using wavelet analysis of surface electromyography (sEMG). *Multi Sci* 12: 1344239. https://doi.org/10.3389/fbioe.2024.1344239
14. Alfaro-Cortés H, García-Manzo R, Ocampo-Estrada B, et al. (2023) Comparing wavelet characterization methods for the classification of upper limb sEMG signals. *Comput Sist* 27: 553–567. https://doi.org/10.13053/cys-27-2-4409
15. Huang N, Shen Z, Long S, et al. (1998) The empirical mode decomposition and the hilbert spectrum for nonlinear and non-stationary time series analysis. *Proc R Soc A Math Phys Eng Sci* 454: 903–995. https://doi.org/10.1098/rspa.1998.0193
16. Zhang P, Lv D, Zhang Y, et al. (2023) Surface electromyogram signal denoising based on boost-CEEMD. *Inf Technol Inf* 7: 176–179. https://doi.org/10.3969/j.issn.1672-9528.2023.07044
17. Koppolu P and Chemmangat K (2023) Automatic selection of IMFs to denoise the sEMG signals using EMD. *J Electromyogr Kinesiol* 73: 102834. https://doi.org/10.1016/j.jelekin.2023.102834
18. Kumar K, Lee D, Jamsrandoj A, et al. (2024) sEMG-based Sarcopenia risk classification using empirical mode decomposition and machine learning algorithms. *Math Biosci Eng* 21: 2901–2921. https://doi.org/10.3934/mbe.2024129
19. Wei C, Wang H, Lu Y, el al. (2022) Recognition of lower limb movements using empirical mode decomposition and k-nearest neighbor entropy estimator with surface electromyogram signals. *Biomed Signal Process Control* 71: 103198. https://doi.org/10.1016/j.bspc.2021.103198
20. Dragomiretskiy K and Zosso D (2014) Variational mode decomposition. *IEEE Trans Signal Process* 62: 531–544. https://doi.org/10.1109/TSP.2013.2288675
21. Xiao F, Yang D, Guo X, et al. (2019) VMD-based denoising methods for surface electromyography signals. *J Neural Eng* 16: 056017. https://doi.org/10.1088/1741-2552/ab33e4
22. Ashraf H, Shafiq U, Sajjad Q, et al. (2023) Variational mode decomposition for surface andintramuscular EMG signal denoising. *Biomed Signal Process Control* 82: 104560. https://doi.org/10.1016/j.bspc.2022.104560
23. Liu Q, Wang S, Dai Y, et al. (2025) Two-dimensional identification of lower limb gait features based on the variational modal decomposition of sEMG signal and convolutional neural network. *Gait Posture* 117: 191–203. https://doi.org/10.1016/j.gaitpost.2024.12.028
24. Prabhavathy T and Elumalai V (2024) Gesture recognition framework for upper-limb prosthetics using entropy features from electromyographic signals and a Gaussian kernel SVM classifier. *Appl Soft Comput* 167: 112382. https://doi.org/10.1016/j.asoc.2024.112382

25. Wen L, Xu J, Li D, et al. (2023) Continuous estimation of upper limb joint angle from sEMG based on multiple decomposition feature and BiLSTM network. *Biomed Signal Process Control* 81: 104303. https://doi.org/10.1016/j.bspc.2022.104303
26. Lu Y, Ma H, Zhang Z, et al. (2024) Real-time chatter detection based on fast recursive variational mode decomposition. *Int J Adv Manuf Technol* 130: 3275–3289. https://doi.org/10.1007/s00170-023-12832-w

AIMS Press